Available online at www.sciencedirect.com

ScienceDirect

Procedia Structural Integrity 37 (2022) 714–721

Structural Integrity Procedia

www.elsevier.com/locate/procedia

ICSI 2021 The 4th International Conference on Structural Integrity

Geometrical parameter study of adhesively-bonded T-joints by cohesive models

J.P.M. Lopes[a], R.G.S.G. Campilho[a,b]*, R.J.B. Rocha[a,b], F.J.G. Silva[a,b]

[a]*ISEP – School of Engineering, Rua Dr. António Bernardino de Almeida, 431, 4200-072 Porto, Portugal*
[b]*INEGI – Pólo FEUP, Rua Dr. Roberto Frias, s/n, 4200-465 Porto, Portugal*

Abstract

A wide variety of adhesive joints architectures is available, offering several options to the designers, although the most common are single-lap joints (SLJ), double-lap joints, and scarf joints. Additional designs, less used and studied are the stepped-lap, *T*-joints and tubular joints. *T*-joints find application in different types of industry, such as aircraft to bond stiffeners to skin and in the cars between the B-pillar and the rocker. This work numerically evaluates the performance of the structural adhesive Araldite® 2015 in an aluminum *T*-joint, after validation with experimental results. A cohesive zone modelling (CZM) numerical study is carried out to capture the behavior of different *T*-joints geometrical configurations when subjected to peel loads. The work includes a parametric study, considering maximum load (P_m) and dissipated energy at failure (U) prediction, considering four geometrical parameters: flat adherend thickness (a), *T*-element thickness (t), overlap length (l) and *T*-element radius (r). A significant effect on P_m was found for the tested parameters, and the CZM method revealed to be a precious method for studying *T* joints with precision and accuracy.

Keywords: Structural adhesive; Adhesive joint; *T*-joint; Cohesive zone model.

1. Introduction

Adhesive bonding is a widely used joining method applied in several fields, from the high-tech aeronautical industry to simpler ones as furniture or shoemaking. It captured the attention of designers due to its outstanding

* Corresponding author. Tel.: +351-939526892; fax: +351-228321159.
E-mail address: raulcampilho@gmail.com

10.1016/j.prostr.2022.02.001

characteristics over other similar joining methods e.g., welding or riveting. In fact, the advantages of this method include the possibility to join different materials while preserving their integrity, since drilling or welding (which causes a heat-affected section) are not necessary. Additionally, it provides more uniform stress distributions, corrosion protection, flexible gap filing and vibration damping (Petrie 2000). Nonetheless, some disadvantages can be attributed e.g., the requirement of a surface treatment prior to adhesive application, disassembly difficulties without damage, low resistance to temperature and humidity, and the need to design the joint oriented towards the elimination of peel (σ_y) stresses. A wide variety of joint architectures is available, offering several options to the designers, although the most common are SLJ, double-lap joints, and scarf joints (Adams 2005), each of them best suited for a certain type of application and load case. *T*-joints find application in different types of industries, such as aircraft to bond stiffeners to skin and in the cars between the B-pillar and the rocker. In the marine industry, *T*-joints can be found in the joints between the bulkheads and the hull in ships. A typical design of this type of joint consists of panels joined by fillet and over laminates. The purpose of a *T*-joint is to transfer flexural, compressive, shear and tensile loads between the leg panel and the base panel (Shenoi et al. 1995). To allow a widespread use, it is important for a designer to have complete knowledge of the joints' strength and failure behavior. Several methodologies are available, and these are mainly divided in two groups, analytical and numerical. Currently, with Finite element method (FEM) analyses, one may easily evaluate intricate structures bonded with highly ductile adhesives(Anyfantis and Tsouvalis 2013, Liao et al. 2014). Few approaches evolved as the continuum or fracture mechanics. Another predictive method, CZM, developed by Barenblatt (1959) and Dugdale (1960), is based on establishing damage laws relating stresses and displacements to induce crack growth along the adhesive layer. The accuracy of this approach requires an exact determination of the cohesive strengths in tension and in shear (t_n^0 and t_s^0, respectively), and the fracture toughness in mode I (G_{IC}) and mode II (G_{IIC}). CZM combined with the FEM proved to be highly accurate for joint strength prediction (Rocha and Campilho 2018).

Different authors addressed *T*-joints (Barzegar et al. 2021). Zhan et al. (2016) investigated the behavior of *T*-joints with different geometries subjected to a tensile loading by using a damage mechanics approach. The aluminum alloy 2060 T8 was selected as adherend and the two-part epoxy EA9394 as adhesive. Experimental tests were performed, allowing to validate the numerical model. The authors found that P_m increases with the increase of the bonding area. In addition, the horizontal bondline has a better ability to increase P_m than the vertical bondline. In fact, it is shown that, by adding a vertical bonding in a *T*-joint, it becomes possible to withstand a very small amount of load comparing with a joint without bonding, while the bondline area increases 123%. Ferreira et al. (2020) performed a CZM numerical analysis to evaluate the behavior of different *T*-joint designs subjected to peel loads. The study focused on the evaluation of the effect of several geometrical parameters on the strength predictions Adherends were made of carbon fibers impregnated with an epoxy resin and bonded with the Araldite® 2015, an epoxy-based structural adhesive. The parametric study included four geometrical parameters: *a*, *t*, *l* and *r* (see Fig. 1 in section 2.1). The authors found that P_m increases by tuning the evaluated parameters as follows: increasing *a,* or reducing *t*. In addition, it was found that *R* only locally affects load transfer near the deltoid. In fact, higher *R* induces higher loads transfer capabilities between the base laminate and the stiffener, therefore improving P_m. The effect of *l* in P_m is advantageous only for *l* between 10 and 20 mm since, above this value, an earlier deltoid failure took place.

This work numerically evaluates the performance of the structural adhesive Araldite® 2015 in an aluminum *T*-joint, after validation with experimental results. A CZM numerical study is carried out to capture the behavior of different *T*-joints geometrical configurations when subjected to peel loads. The work includes a parametric study, considering P_m and *U* prediction, considering four geometrical parameters: *a*, *t*, *l* and *r*.

2. Materials and methods

2.1. T-joint geometry

Fig. 1 presents the *T*-joint design and its dimensions. The baseline geometry includes (in mm): length L_T=200, *T*-element free length L_A=40, width *B*=25, *a*=3, *t*=1.5, *l*=30, *r*=6 and adhesive thickness (t_A)=0.2. A study will be performed to evaluate the geometric influence of the most relevant dimensional parameters on the joint strength, by comparing with the baseline performance. The following parameters are affected: *a* (1, 2, 3 and 4 mm), *t* (0.5, 1, 1.5, 2 and 2.5 mm), *l* (10, 20, 30 and 40 mm) and *r* (3, 6, 9 and 12 mm).

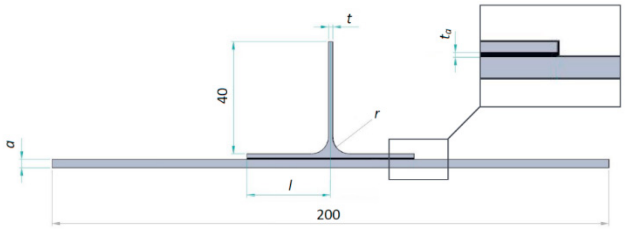

Fig. 1. T-joint geometry and dimensions.

2.2. Materials

The medium strength aluminum alloy AW 6082-T651 was selected as adherend material mainly due to its common use in structural applications. The characterization of this alloy in bulk tension is detailed in an earlier work (Moreira and Campilho 2015). The estimated aluminum properties are: Young's modulus (E) of 70.07±0.83 GPa, tensile yield stress (σ_y) of 261.67±7.65 MPa, tensile strength (σ_f) of 324±0.16 MPa and tensile failure strain (ε_f) of 21.70±4.24%. The Araldite® 2015, an epoxy ductile adhesive, was considered to execute the joints. The mechanical and fracture characterization of the Araldite® 2015 are included in a previous work (Campilho et al. 2013). The tensile mechanical properties were defined by tensile tests to bulk specimens. In addition, Thick Adherend Shear Tests were used to estimate the shear mechanical properties. The relevant fracture properties of the adhesive (G_{IC} and G_{IIC}) were obtained from Double-Cantilever Beam and End-Notched Flexure tests, respectively. The adhesive properties used to feed the numerical model are described in Table 1.

Table 1. Properties of the adhesives Araldite® 2015 (Campilho et al. 2013).

Young's modulus, E [GPa]	1.85±0.21	Shear yield stress, τ_y [MPa]	14.6±1.3
Poisson's ratio, ν	0.33	Shear failure strength, τ_f [MPa]	17.9±1.8
Tensile yield stress, σ_y [MPa]	12.63±0.61	Shear failure strain, γ_f [%]	43.9±3.4
Tensile failure strength, σ_f [MPa]	21.63±1.61	Toughness in tension, G_{IC} [N/mm]	0.43±0.02
Tensile failure strain, ε_f [%]	4.77±0.15	Toughness in shear, G_{IIC} [N/mm]	4.70±0.34
Shear modulus, G [GPa]	0.56±0.21		

2.3. Numerical conditions

In order to study the geometrical effect in T-joints subjected to peel loads, and using CZM, the Abaqus® software was used. The base model was built with vertical symmetry conditions. Two-dimensional models were considered because the geometry has a constant section outside the plane (Kafkalidis and Thouless 2002). The joint geometry was divided into partitions to facilitate the construction of the mesh. The aluminum adherends were modelled with 4-node plane-strain isotropic elements with the reference CPE4 (Campilho et al. 2011). On the other hand, the adhesive layer was replaced in the models by 4-node cohesive elements (with the reference COH2D4) using one layer of elements through-thickness. The mesh refinement is presented in Fig. 2 (a) and the boundary conditions in Fig. 2 (b). For the adhesive layer, a cohesive-type section with cohesive material properties with t_A=0.2 mm was considered, while the aluminum portion was modelled with a solid and homogeneous section (Tzetzis and Hogg 2008). Finally, the boundary conditions applied to the structure consisted of clamping one edge of the T adherend and applying a vertical displacement at the top. As previously mentioned, a vertical symmetry condition was inducted in the mid-plane of the structure.

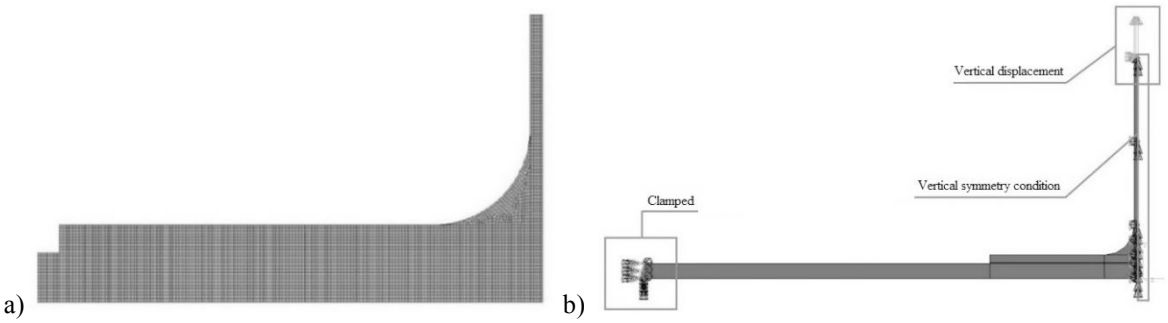

Fig. 2. Example of mesh refinement at the overlap region (a) and boundary conditions applied to the numerical models (b).

2.4. CZM theory

CZM laws rely on relationships correlating stresses with displacements, which link paired nodes of the CZM finite elements. These laws are typically divided into two regions: elastic stress evolution until reaching the maximum load, and material degradation, induced by a stiffness loss, to model the failure process (Anyfantis and Tsouvalis 2012). The area under the tension and shear traction-separation laws is the respective fracture toughness (G_C) of the material. In pure mode (tensile or shear), crack growth takes place after the stresses being released in the corresponding CZM law. In mixed mode, it is necessary to used specific criteria to combine the pure modes (Alfano 2006). The present work is based on triangular pure and mixed-mode laws, in which material degradation is linear up to failure. The linear elastic portion of the CZM law is established by an elastic matrix combining stresses and strains, and depending on E and the shear modulus (G_{xy}). The quadratic stress criterion was used as limit of the elastic part. After reaching the mixed-mode cohesive strength (t_m^0), material degradation begins. Failure is assessed by a linear criterion based on G_C. This model is described in detail elsewhere (Campilho et al. 2012). Table 1 collects the CZM data.

3. Results

3.1. Validation with experiments

Before the *T*-joint numerical optimization by CZM, a previous validation is performed using a double-*L T*-joint with the same materials, i.e., practically the same geometry but with the difference that the *T*-part is built from two bent adherends glued along the rib region. The geometry of this validation joint is presented in Fig. 3. The loading and boundary conditions are identical to the geometry of this work. The dimensions of the validation *T*-joint are (in mm): l=25, width B=25, L_T=80, a=3, t=1, 2, 3 and 4, L_A=60, r=5 and t_A=0.2.

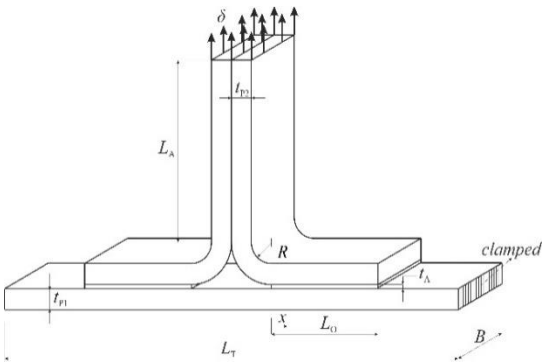

Fig. 3. Geometry of the double-*L T*-joints for validation purposes.

These joints were fabricated by cutting the adherends and bending the *L*-shaped adherends, followed by surface preparation by grit blasting. Curing was undertaken in an in-house jig to guarantee the joint parts' alignment, while steel spacers were inserted at the overlap edges to achieve t_A=0.2 mm and, finally, individual application of pressure on the bonded areas with grips (Campilho et al. 2011). Curing was developed during an entire week. The *T*-joints were peel-tested at room temperature and with 1 mm/min in a Shimadzu AG-X 100 tester equipment and using a 100 kN load cell. Five specimens were tested for each *t*, to produce an average P_m and respective standard deviation. The numerical premises were identical to those described in section 2.3, including the dimensional approach (two-dimensional), element types, triangular CZM, boundary conditions, mesh topology and refinement, including the consideration of bias effects for time saving (Fernandes et al. 2015). The tests revealed a cohesive failure of the adhesive for all specimens. Fig. 4 depicts the experimental average/deviation of P_m and respective CZM predictions.

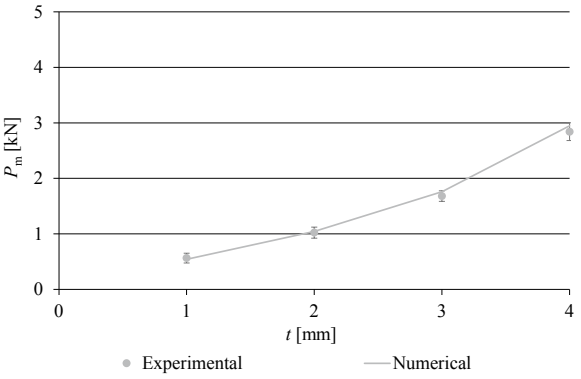

Fig. 4. Experimental and CZM comparison as a function of *t*.

The experimental data shows a clear effect of *t* on P_m, in the sense that a marked P_m increase takes place with this parameter, which emphasis to the marked improvement between *t*=3 and 4 mm. For this specific adhesive, the P_m improvement for the different *t* over the *t*=1 mm condition is 81.2% (2 mm), 197.8% (3 mm) and 403.7% (4 mm), which constitutes a marked performance improvement, and it is related to the flexibility and ductile nature of this epoxy adhesive. Actually, adhesives with these characteristics are able to afford more uniform σ_y and shear (τ_{xy}) stresses in the adhesive layer and reduce peak stresses. On the other hand, they undergo the plastic regime before failing, and the transmitted stresses are higher. This behavior takes place because of a higher extension of the plastic length induced by higher G_{IC} and G_{IIC} than with brittle adhesives. The P_m comparison for the *T*-joints bonded with the adhesive Araldite® 2015 showed a close agreement between the CZM results and the experiments. However, P_m was over predicted for all *t* apart from 1 mm (difference of 4.3%). On the other hand, the experimental P_m for *t*=2, 3 and 4 mm were below the CZM values by 2.2%, 4.5% and 3.5%, respectively. These results confirm that the proposed numerical method is reliable for the numerical study that follows.

3.2. Joint strength

This section presents the results of the joint strength for all geometrical parameters. All the data result from the load-displacement (P–δ) curves obtained with Abaqus®. The effects are discussed individually by parameter:

- The P_m results highly depend on *a* (Fig. 5 a). As it can be seen, increasing *a* results in higher P_m. The relative P_m improvement between *a*=1 and 4 mm was 112.8%. This behavior is due to the increased stiffness of the base. On the other hand, increasing *a* decreases the failure displacement due to the corresponding joints' stiffness improvement;

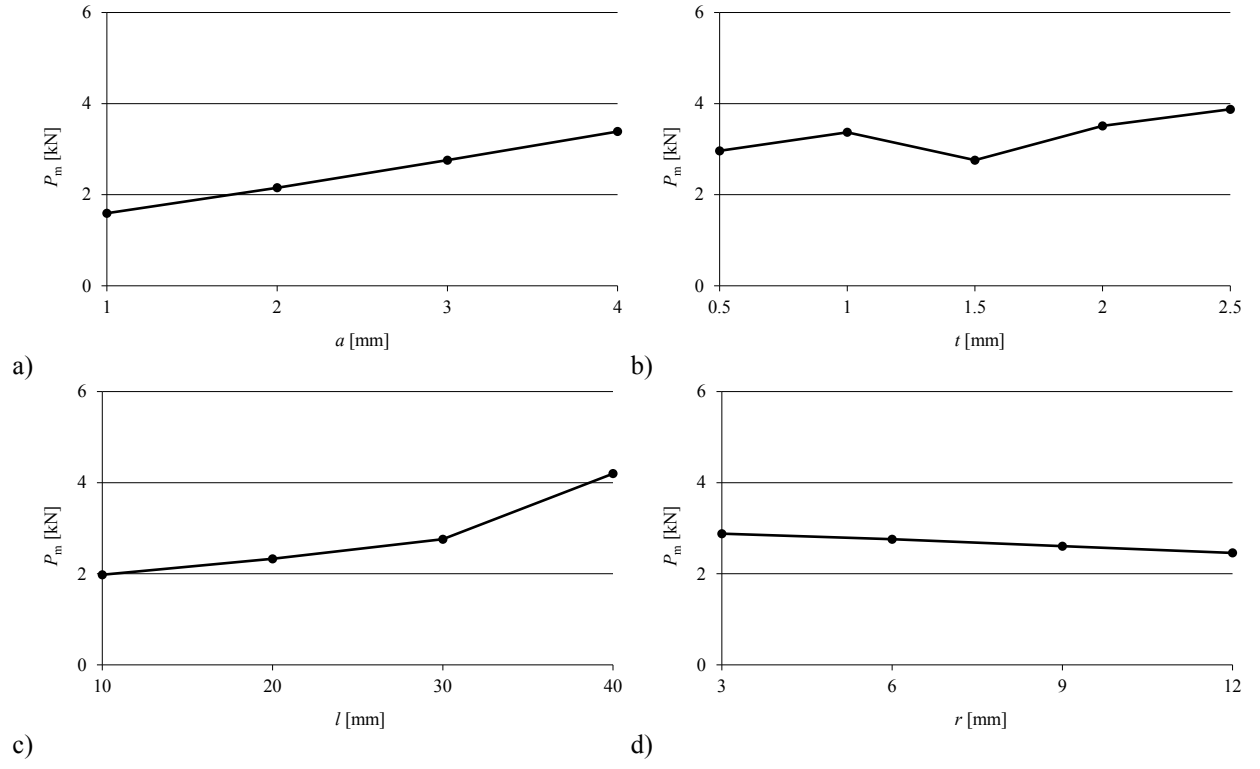

Fig. 5. P_m for the different parameters: a (a), t (b), l (c) and r (d).

- With the increase of t, P_m also increases (Fig. 5 b). The P_m improvement between t=0.5 and 2.5 mm was found to be 30.8 %. There was, however, an exception in the P_m evolution for t=1.5 mm, which registered a lower value than expected. In the numerical analyses, a difference was found in the failure mode for t=0.5 and t=1 mm compared to t=1.5, 2 and 2.5 mm, which explained the odd P_m evolution. Actually, in the first case, failure occurred near to x/l=0.8, and in the second case at x/l=0. For t> 1.5 mm there was an increase in P_m up to t=2.5 mm. Regarding the failure displacement, slightly higher values were registered for higher t, which is justified by the bigger attained P_m;
- By increasing the values of l, P_m increases in a sustained manner (Fig. 5 c), with a difference of 112.2% between limit l values. Using the ductile adhesive selected for this work, the increase of l leads to a larger plasticized area and, consequently, to higher levels of transmitted stresses through the adhesive layer. As a result, P_m steadily increases as well. The highest P_m increase was found between l=30 and 40 mm;
- The P_m-r results are presented in Fig. 5 (d). It was found that P_m increases linearly with the decrease of r (up to 17.2% between r=3 and 12 mm). Regarding the failure displacement, it progressively decreases with the increase in r values due to the higher T stiffness.

3.3. Dissipated energy

This section aims to study the energy dissipation at failure (U) for the T-joints with the various geometries. This parameter was calculated by the numerical P-δ curves provided by Abaqus®, using the area below the respective P-δ curve, which in turn was estimated by discrete integration functions in Excel®. All analyses were based on the initial dimensions (a=3 mm, l=30 mm, t=1.5 mm and r=6 mm), only varying the parameter under analysis. Fig. 6 collects all U data as a function of the chosen dimensions for each parameter. Each effect is discussed separately.

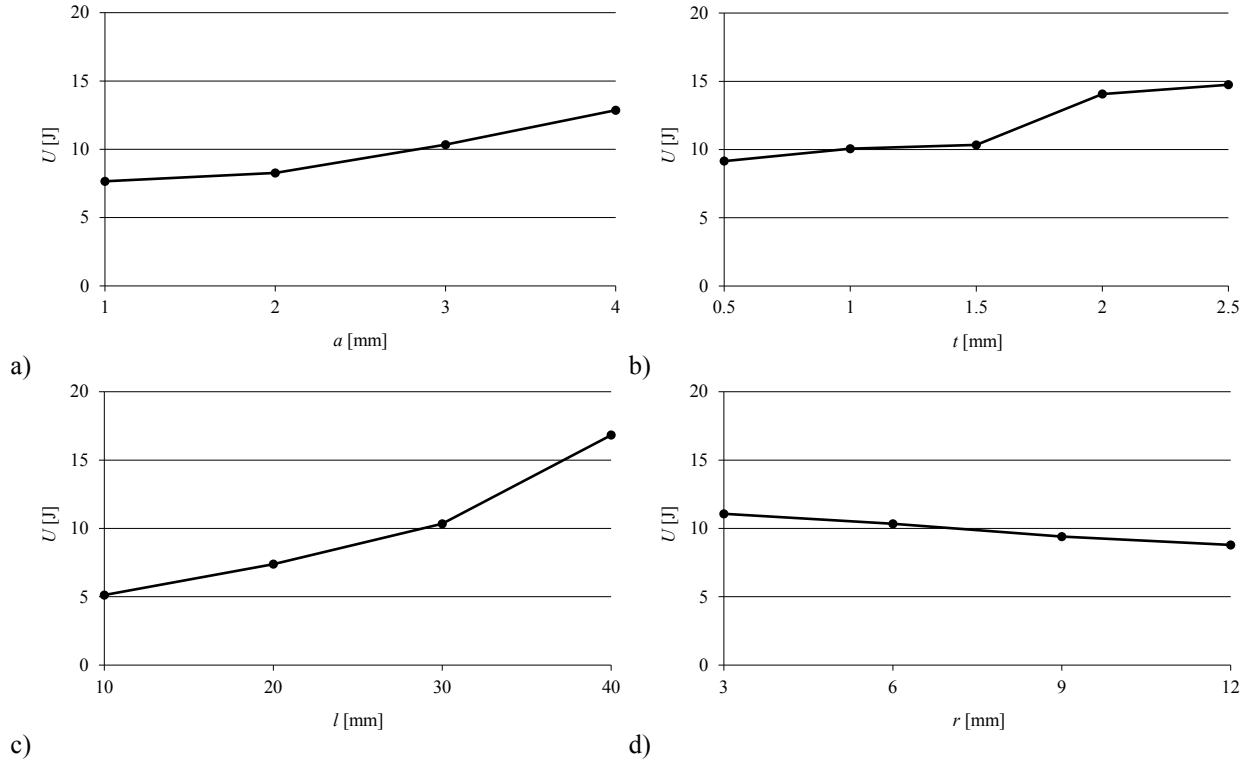

Fig. 6. U for the different parameters: a (a), t (b), l (c) and r (d).

- The effect of a (Fig. 6 a) is notorious, with a steady increasing tendency of U with this parameter, especially for a>2 mm. The percentile improvements over a=1 mm were 8.0% (a=2 mm), 35.0% (a=3 mm) and 67.9% (a=4 mm). This behavior is closely related with increasing base stiffness of the T-joint that, although reducing the failure displacement of the joint, highly increases P_m, thus rendering higher U. As a result of this analysis, a is considered to be a primordial design parameter under the scope of both P_m and U;
- The influence of t (Fig. 6 b) is somehow analogous to that of a, but the tendency is far from linear. Actually, a U improvement was found, although only being significant between t=1.5 and 2 mm. The relative improvement over t=0.5 mm (smallest considered value) was 9.9%, 13.0%, 57.7% and 61.1% using t from 1 mm to 2.5 mm. Identically to the previous geometric parameter, this improvement is related to the higher loads and displacements to failure induced by the higher T-part stiffness and improved load transfer between joint components;
- l is traditionally one of the most significant parameters for generic strength improvement of bonded joints, and this behavior also reflected on the T-joints (Fig. 6 c). Actually, unlike other geometric modifications, l directly impacts the amount of adhesive available to transmit the loads. The percentile improvements of P_m with l, starting from l=10 mm, were 44.1%, 101.7% and 228.3%, up to l=40 mm. This major improvement is made possible due to the ductility of this particular adhesive.
- The r parameter (Fig. 6 d) has a significant effect on U, but with higher r decreasing P_m in an approximately linear manner for the tested values in this work. The best results were thus found for r=3 mm. For bigger values, percentile depreciations of 6.6% (r=6 mm), 15.0% (r=9 mm) and 20.6% (r=12 mm) were found. The smaller efficiency with higher r is related to premature failures of the adhesive layer due to the stiffer reinforcement, which then triggers premature failure.

4. Conclusions

This work aimed to numerically study, by CZM, the behavior of *T*-adhesive joints between aluminum adherends, considering different geometric variables (*a*, *t*, *l* and *r*). Numerically, a P_m and *U* analysis was performed, using the Abaqus® software. Visible differences were found depending on the geometrical parameters, which then translated into different P_m and *U*:

- *a* effect: Increasing *a* value showed an P_m and *U* improvement and this behavior was due to the increased stiffness of the base. This analysis revealed *a* as an important design parameter;
- *t* effect: Increasing the *t* thickness, a P_m improvement was observed between *t*=0.5 and 2.5 mm, with an exception for *t*=1.5 mm with a lower value. The *t* influence in *U* study was somehow analogous to that of *a*, but not linear;
- *l* effect: Due to the ductility of this adhesive, increasing the *l* value leads to a larger plasticized area and, consequently, P_m and *U* increase accordingly;
- *r* effect: It was found that P_m increases linearly with the decrease of *r*. On the other hand, the *r* parameter has a significant effect on *U*, with higher *r* decreasing *U* in an approximately linear manner for the tested values.

In conclusion, *a* proved to be the most important parameter in this type of reinforcement joint, and CZM method revealed to be a precious FEM method for studying *T* joints with precision and accuracy.

References

Adams, R. D. (2005). Adhesive bonding: science, technology and applications, Elsevier.

Alfano, G., 2006. On the influence of the shape of the interface law on the application of cohesive-zone models. Composites Science and Technology 66(6), 723-730.

Anyfantis, K. N. and Tsouvalis, N. G., 2012. A novel traction–separation law for the prediction of the mixed mode response of ductile adhesive joints. International Journal of Solids and Structures 49(1), 213-226.

Anyfantis, K. N. and Tsouvalis, N. G., 2013. A 3D ductile constitutive mixed-mode model of cohesive elements for the finite element analysis of adhesive joints. Journal of Adhesion Science and Technology 27(10), 1146-1178.

Barenblatt, G. I., 1959. The formation of equilibrium cracks during brittle fracture. General ideas and hypotheses. Axially-symmetric cracks. Journal of Applied Mathematics and Mechanics 23(3), 622-636.

Barzegar, M., Moallem, M. D. and Mokhtari, M., 2021. Progressive damage analysis of an adhesively bonded composite T-joint under bending, considering micro-scale effects of fiber volume fraction of adherends. Composite Structures 258, 113374.

Campilho, R. D. S. G., Banea, M. D., Chaves, F. J. P. and Silva, L. F. M. d., 2011. eXtended Finite Element Method for fracture characterization of adhesive joints in pure mode I. Computational Materials Science 50(4), 1543-1549.

Campilho, R. D. S. G., Banea, M. D., Neto, J. A. B. P. and da Silva, L. F. M., 2012. Modelling of single-lap joints using cohesive zone models: Effect of the cohesive parameters on the output of the simulations. The Journal of Adhesion 88(4-6), 513-533.

Campilho, R. D. S. G., Banea, M. D., Neto, J. A. B. P. and da Silva, L. F. M., 2013. Modelling adhesive joints with cohesive zone models: effect of the cohesive law shape of the adhesive layer. International Journal of Adhesion and Adhesives 44, 48-56.

Campilho, R. D. S. G., Banea, M. D., Pinto, A. M. G., da Silva, L. F. M. and de Jesus, A. M. P., 2011. Strength prediction of single- and double-lap joints by standard and extended finite element modelling. International Journal of Adhesion and Adhesives 31(5), 363-372.

Dugdale, D. S., 1960. Yielding of steel sheets containing slits. Journal of the Mechanics and Physics of Solids 8(2), 100-104.

Fernandes, T. A. B., Campilho, R. D. S. G., Banea, M. D. and da Silva, L. F. M., 2015. Adhesive selection for single lap bonded joints: Experimentation and advanced techniques for strength prediction. The Journal of Adhesion 91(10-11), 841-862.

Ferreira, J. A. M., Campilho, R. D. S. G., Cardoso, M. G. and Silva, F. J. G., 2020. Numerical simulation of adhesively-bonded T-stiffeners by cohesive zone models. Procedia Manufacturing 51, 870-877.

Kafkalidis, M. S. and Thouless, M. D., 2002. The effects of geometry and material properties on the fracture of single lap-shear joints. International Journal of Solids and Structures 39(17), 4367-4383.

Liao, L., Sawa, T. and Huang, C., 2014. Numerical analysis on load-bearing capacity and damage of double scarf adhesive joints subjected to combined loadings of tension and bending. International Journal of Adhesion and Adhesives 53, 65-71.

Moreira, R. D. F. and Campilho, R. D. S. G., 2015. Strength improvement of adhesively-bonded scarf repairs in aluminium structures with external reinforcements. Engineering Structures 101, 99-110.

Petrie, E. M. (2000). Handbook of adhesives and sealants. New York, USA, McGraw-Hill.

Rocha, R. J. B. and Campilho, R. D. S. G., 2018. Evaluation of different modelling conditions in the cohesive zone analysis of single-lap bonded joints. The Journal of Adhesion 94(7), 562-582.

Shenoi, R. A., Read, P. J. C. L. and Hawkins, G. L., 1995. Fatigue failure mechanisms in fibre-reinforced plastic laminated tee joints. International Journal of Fatigue 17(6), 415-426.

Tzetzis, D. and Hogg, P. J., 2008. Experimental and finite element analysis on the performance of vacuum-assisted resin infused single scarf repairs. Materials & Design 29(2), 436-449.

Zhan, X., Gu, C., Wu, H., Liu, H., Chen, J., Chen, J. and Wei, Y., 2016. Experimental and numerical analysis on the strength of 2060 Al–Li alloy adhesively bonded T joints. International Journal of Adhesion and Adhesives 65, 79-87.